Journal of Manufacturing Processes 34 (2018) 793–801

Contents lists available at ScienceDirect

Journal of Manufacturing Processes

journal homepage: www.elsevier.com/locate/manpro

A vibration-assisted method to reduce separation force for stereolithography

Jie Jin[a], Jingfan Yang[b], Huachao Mao[a], Yong Chen[a,*]

[a] Daniel J. Epstein Department of Industrial and Systems Engineering, University of Southern California, Los Angeles, CA, 90089, USA
[b] Mork Family Department of Chemical Engineering and Materials Science, University of Southern California, Los Angeles, CA, 90089, USA

ARTICLE INFO

Keywords:
Stereolithography
Additive manufacturing
Vibration
Separation force
Frequencey

ABSTRACT

Current stereolithography (SL) technology can print layer-based three-dimensional (3D) objects with high precision and fast speed. However, for a constrained surface based top-down or bottom-up SL process, it will be very difficult to separate the building layers from the constrained glass due to the near vacuum environment between the built layer and the constrained glass. The separation force will significantly increase when the contact area increases. Current existing methods to address this problem include tilting the vat, sliding the vat, and adopting the oxygen permeable membrane. However, the construction complexity and cost of the building systems will increase significantly with the increase of the maximum area that the system can build using the existing methods. In this paper, a novel separation method for the SL process utilizing a vibration-assisted glass is presented. A pair of general loudspeakers were used to provide a low frequency vibration for the constrained glass used in the SL process. Two force sensors are used to measure the separation force in real time. Controlled experiments have been implemented and the corresponding data was collected and analyzed. The analyzed results have demonstrated that the proposed method can significantly reduce the separation force for the SL process. Two test cases are presented to show the effectiveness of the presented vibration-assisted SL process.

1. Introduction

Additive manufacturing (AM), also known as 3D printing, or rapid prototyping/manufacturing, refers to process used to make a three-dimension object in a layer-by-layer manner [1]. The shape of each layer can be dynamically controlled by a computer-aided design (CAD) system. The advantages of AM, compared with traditional subtractive manufacturing technologies, include reducing material waste, simplifying manufacturing process and are not limited by geometrical complexity [2,3].

As the first commercialized AM technology, SL process is one of the most popular AM technologies. In SL process, the liquid photosensitive polymer is solidified by a pattern controllable irradiation light source such as a digital light processing (DLP) projector or a laser beam [4–6]. Compared to other polymer AM techniques such as extrusion or jetting processes, SL produces parts with the higher accuracy, the best surface quality and faster building speed [7–13]. Basically, there are two kinds of SLA processes based on different resin filling mechanisms: free surface method and constrained surface method [8]. For free surface method, the polymer is directly exposed to irradiation light and solidified. As for the constrained surface method, the top-down or bottom-up method is used to build a part. The photosensitive polymer is always sandwiched between the building surface and the constrained surface. Contrast to the free surface method, the platform needs to move up and down to let polymer refill into the gap between the building surface and the constrained surface.

Compared to the free surface method, the constrained surface process has several advantages, such as higher vertical dimensional accuracy, higher material filling rate, and faster building speed, etc. More importantly, by controlling moving distance of platform, part with thinner layer can be achieved. However, there are still many problems existing for this constrained surface method. It is very difficult to separate the newly cured layer from the constrained surface. This difficulty results from an adhesive bonding that is developed between the newly cured layer and the constrained surface. Thus, a separation force is needed to separate the built part from the constrained surface. Such a separation force will significantly affect the printing speed, reliability of printing process, printable size and life cycle of the constrained surface [14–16].

1.1. Challenges faced in separation based SL process

The existing separation problem in constrained surface SL process has blocked the development of 3D printing in a large scale of building area.

To solve this problem, many attempts have been made [17,18]. The

* Corresponding author.
E-mail address: yongchen@usc.edu (Y. Chen).

https://doi.org/10.1016/j.jmapro.2018.03.052
Received 1 December 2017; Received in revised form 5 March 2018; Accepted 15 March 2018
Available online 29 May 2018

most common way to address this problem is making a non-sticky and air-permeable coating on constrained surface such as using Teflon films or polydimethylsiloxane (PDMS) [19]. However, the force required to separate the cured layer from the PDMS-coated constrained surface is still considerably large. EnvisionTEC Inc. developed another approach based on a peeling mechanism, aiming to reduce the separation force as the force required for peeling is much less than pulling. To facilitate the peeling process, a tilting motion system was adopted by lifting or lowering one side of the platform slowly while pivoting it about the other side. However, this mechanism performs poorly for a part with large cross-section area as the designed tilting angle is coupled with the maximum building area the process can deal with. Furthermore, the additional tilting motion increases the fabrication time resulting in reduction of the productivity. Another mechanism was developed based on the peeling approach using a two-channel system [7]. This method is aimed at changing the pull-up force into shear force. During the horizontal translation, the built part gets separated from the resin vat, facilitating convenient vertical motion of the platform by a pulling-up action. However, the disadvantage of this two-channel approach is that the area of the vat should always be designed at least double size of the maximum building area resulting in increased construction complexity as the building area increases.

An unprecedented method based on the continuous liquid interface production process was proposed [20]. In this method, a highly air permeable coating was used to increase the oxygen concentration below the constrained surface. Despite its advancement, it is still a significant challenge when it comes to a part with a large contact surface area because the separation force will be extremely large even though the separation force is inversely proportional to the thickness of the dead zone.

Although various methods have been proposed based on the surface treatment or the intelligent design of motions for the building vat, the barrier has never been completely solved.

1.2. Contributions

To address the limitations in constrained surface SL process, we present a novel approach aiming to utilize the vibration in a low frequency to separate the newly cured surface from the constrained surface with a minimum incremental construction complexity as the building area increases. Our approach is a constrained surface SL process based on a top-down projection system. An experimental prototype is presented in Section 2. Experimental comparisons have verified the effectiveness of the proposed approach in significantly reducing the separation force. Consequently, the developed vibration-assisted SL process is promising to fabricate parts with a large cross-sectional area.

2. Design of the vibration-assisted system

In this research, a top-down mask-image-projection based stereolithography (MIP-SL) process is applied to build desired parts. However, unlike the traditional top-down SL process in which the top resin surface is constrained by a fixed transparent glass, a Teflon-coated transparent glass is mounted on two aluminum bars which can vibrate along with the vibration of the membrane in the paper cone of the loudspeaker (*MB42X, Micca Inc.*). Instead of using a direct-pull method to separate the built surface and the glass after certain exposure time, we enable the vibration of the glass to break the vacuum environment between the built surface and the glass, which can facilitate the surface separation.

2.1. Experimental hardware system

A prototype system has been built to study the effect of the vibration to reduce the separation force. The hardware setup of the vibration-assisted SL system is shown in Fig. 1. In the designed system, an ultraviolet(UV) light projector is used. The wavelength of the light source is 405 nm. The power consuming of the light source is ~7 W. The projection resolution of the projector is 1280 × 800. The material we used in our experiments is Makerjuice G+. As shown in the Fig. 1, two ends of the glass are mounted on two aluminum frames, respectively. The other end of the aluminum frames is mounted on the paper cone of the loudspeaker. The paper cone of the loudspeaker can deform within a certain degree. When there is a certain electrical signal transmitted into the speaker, it will cause the paper cone to vibrate and finally transmit the vibration to the glass window mounted on the aluminum frames. Different frequencies of the signal will cause various amplitudes of the vibration due to resonance. In our experiments, we used a sine wave as the input signal and the most effective frequency we have tested in our experiments is 60 Hz with a 50% of the maximum volume. An artificial boundary wall was added to prevent resin filling into the top surface of the glass window as shown in Fig. 1.

Two pressure sensors were fixed on the top flat surface of the loudspeakers as shown in Fig. 1. Right above the pressure sensors there are two vertical aluminum bars mounted on the aluminum frames which can vibrate along with the vibration of the paper cone of the loudspeaker. Two fixtures were mounted in the bottom end of the vertical aluminum bars. A steel spring was used to connect a round flat pad and the fixture mounted on the vertical aluminum bar. The purpose of using a steel spring here is to store energy when there is a vibration caused by the paper cone of the loudspeaker and the spring will be compressed or released at that moment. But it will not influence the maximum value of the pressure force applied on the pressure sensor from the round flat pad above. It can also filter out the noise data caused by the vibration as the similar concept we learned from the design of the capacitor in the electrical circuit.

As shown in Fig. 2, the top building layer of liquid resin will be solidified after certain exposure time of a mask image. Thus, a vacuum environment is formed between the top surface of the building part and the bottom surface of the constrained glass. If we try to move down the building platform to separate the building surface and the glass, the separation force will be extremely big when a large area of the resin is solidified. Let $\boldsymbol{f}_{separation}$ denotes the separation force as shown in Fig. 2. Due to the deformation of the paper cone of the loudspeaker, the constrained glass will be pulled down a certain distance until which moment the vacuum environment breaks and the top building surface detaches from the constrained glass. It will also cause a downward displacement of the vertical aluminum bar during this period as shown in Fig. 2. The paper cone here at this moment can be treated as a hinge for simplification. Meanwhile, the spring mounted in the bottom end of the vertical aluminum bar will be gradually compressed and it will cause an increasing pressure force applied on the pressure force sensor below. As shown in Fig. 2, let $\boldsymbol{f}_{LLift}$ denotes the vertical lift force the aluminum bar A applies on the glass. Likewise, $\boldsymbol{f}_{RLift}$ denotes the vertical lift force the aluminum bar B applies on the glass. Let $\boldsymbol{f}_{LPush}$ and $\boldsymbol{f}_{RPush}$ denote the horizontal force the aluminum bar A and B applied on the glass, respectively. From the force balancing, we will have the following equations,

$$\begin{aligned} |\boldsymbol{f}_{separation}| &= |\boldsymbol{f}_{LLift}| + |\boldsymbol{f}_{RLift}| \\ \boldsymbol{f}_{LPush} &+ \boldsymbol{f}_{RPush} = 0 \end{aligned} \tag{1}$$

2.2. Calibration for the pressure force sensor

Fig. 3 shows the electrical schematics of the application of the pressure sensor (*Pololu Inc., Las Vegas*) we used in our experiments. The chosen pressure sensor is a force-sensitive resistor. The resistance will change along with the change of the pressure force applied on the sensor.

As shown in Fig. 3, the analog/digital converter in the microcontroller is using a 10-bits register which means the raw data obtained

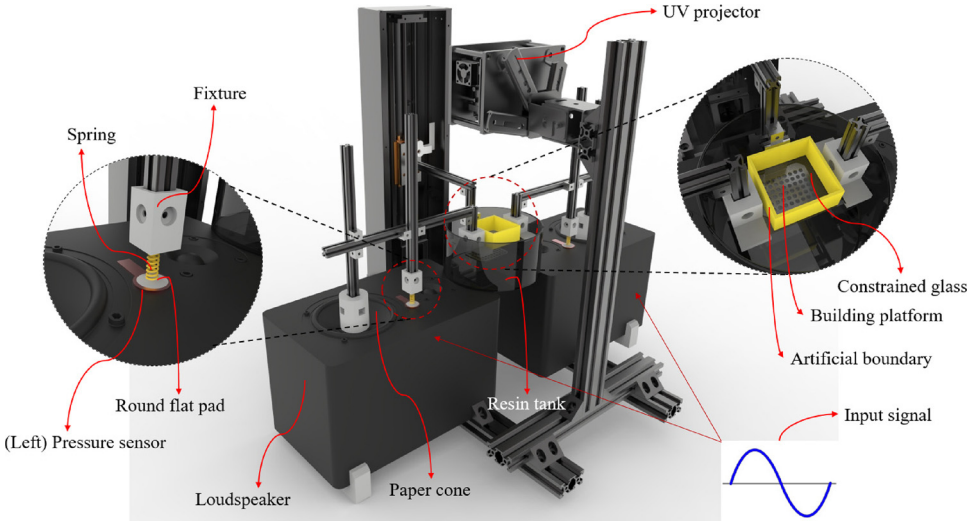

Fig. 1. The hardware setup of the vibration-assisted system.

from the sensor ranges from 0 to 1024. Obviously, the data we read from the sensor does not have a linear relationship with the resistance of the sensor and the relationship between the resistance of the sensor and the real pressure force sensed is unknown.

To establish the relationship between the reading and actual force, the calibration as shown in Fig. 4 was performed. We used screws as a standard weight. We assumed the weight should be always consistent for the same type of screws. We added the weight at the point A where there would be a vertical pulling force applied during the printing process as shown in Fig. 2. We gradually added the weight with certain increment. The total weight and the corresponding data value read from the sensor are recorded.

By using the above calibration method, we obtained 16 pairs of data from the calibration experiments. Then we utilized the relationship between the data read from the sensor and the real force to plot two scatter diagrams, which were left sensor read vs. real force and right sensor read vs. real force as shown in Fig. 5a and b.

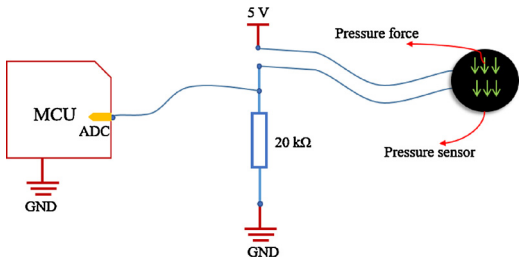

Fig. 3. A schematic of using a pressure force sensor.

After analyzing the trend of these scatter points, we found that there could be a logarithmic relationship between the data read from the sensor and the real force. Hence, we decided to use nature logarithmic

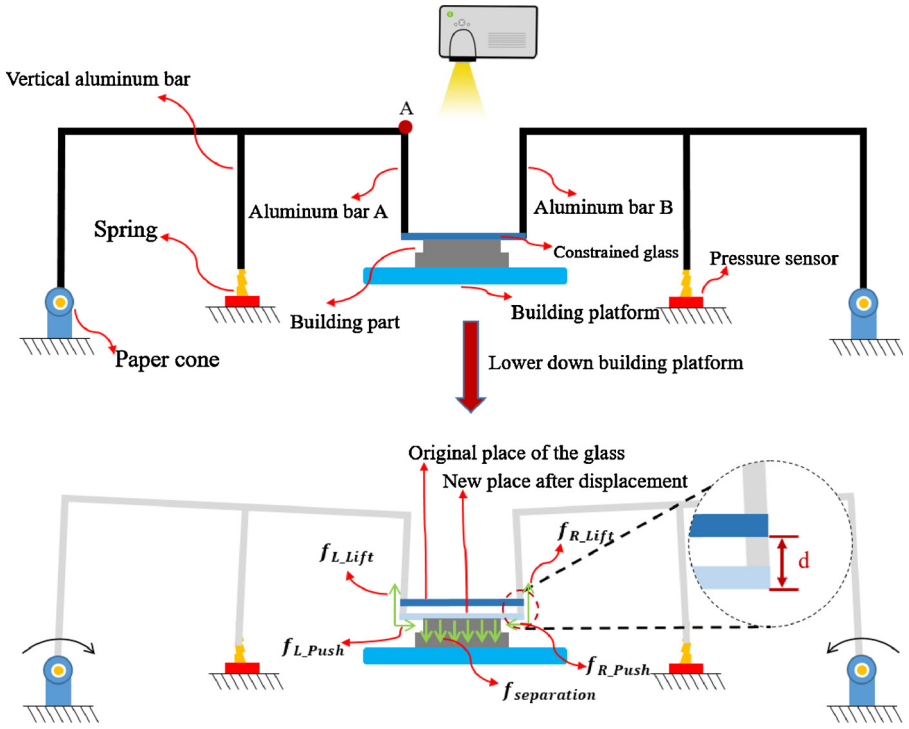

Fig. 2. The illustration of the separation force measurement.

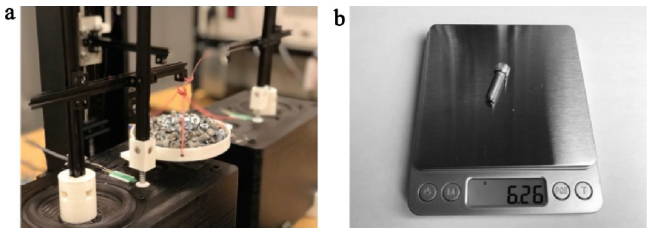

Fig. 4. (a) Weights added to calibrate the sensor; and (b) using screws as standard weights.

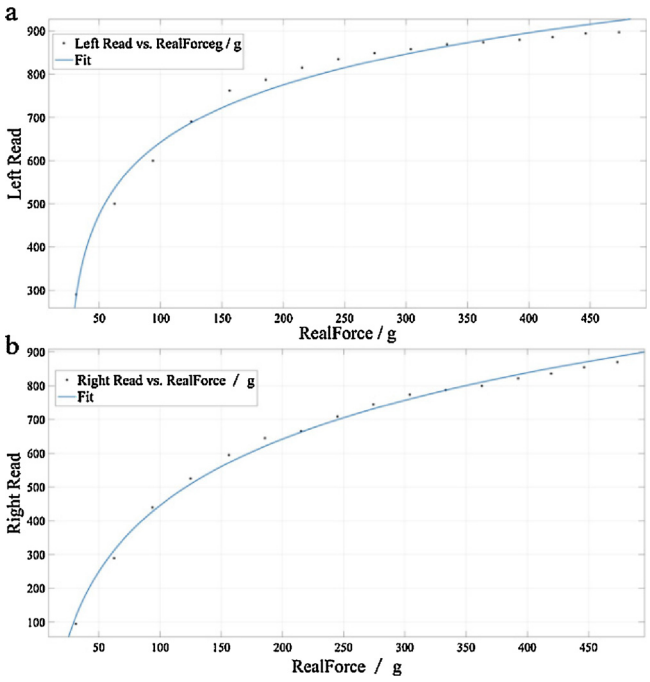

Fig. 5. Calibration results for the corresponding force sensors. (a) Left force sensor calibrated; and (b) right force sensor calibrated.

function to fit these scatter points. We utilized Curve Fitting Tool from MATLAB R2016a to get our fitting curves as shown in Fig. 5. The fitted function is shown as follows.

$$f_R(x) = 283.5log(x) - 859.8 \quad (2)$$

The R-square here is equal to 0.9942, which is acceptable and it also means that the basic equation we used can fit these scatter points perfectly.

Likewise, we got the fitted function for the left sensor as follows.

$$f_L(x) = 159.3log(x - 23.15) - 49.08 \quad (3)$$

The corresponding R-square is 0.9836.

3. Analysis of experimental data and modeling

In this section, we implemented the controlled experiments to study the effect of glass vibration to the separation force. A CAD model with different sections of area was designed to study the relationship between the printing cross-sectional area and the separation force and the difference between using glass vibration and without using glass vibration. The data from left and right pressure sensors was collected and analyzed in both macro and micro manners. A mathematical model was established to illustrate the vibration based separation process.

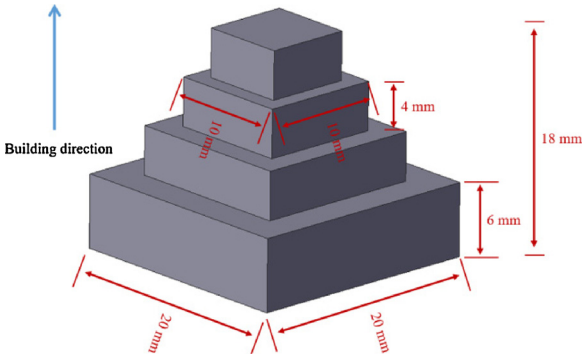

Fig. 6. CAD model used in our experiments.

3.1. Design of the experimental CAD model

As shown in Fig. 6, a CAD model with four different sections of area was designed. The dimensional size was labeled in Fig. 6. Basically, the cross-sectional shape of each section was a square and the cross-sectional area was halved section by section. The reason we integrated the four different areas in a single model rather than four different models with different cross-sectional area was because we wanted to eliminate the unexpected data error between experiments caused by frequently adjust the hardware setup to achieve the exactly the same level of the flat pad above the pressure sensor as shown in Fig. 1. We assume the setup configuration would keep consistent during a single experiment.

The designed layer thickness was 100 μm and we had 60 layers for the base section and 40 layers for each of other three sections. The extra 20 more layers for the base section was to eliminate the influence of over compression in the first several building layers.

3.2. Design of printing process

In our experiments, we designed the printing process in the following manner. First of all, we tried to build 40 layers for the base section using normal method which means we disabled the vibration for the glass and just directly moved down the platform to separate the building surface with the constrained glass after a certain exposure time. The exposure time in our experiments was set as 40 s for the first three layers and 12 s for the other layers. After that, we built another 20 layers for the base section with the glass vibration enabled. Then the fabrication for the second section began. We disabled the glass vibration in the first 20 layers for the second section and enabled it the latter 20 layers. Likewise, the fabrication processes used for the third and fourth sections were the same as the second one's. The flow chart of the designed printing process is shown as Fig. 7.

3.3. Acquisition and analysis of experimental data

We sampled the data at a constant rate of 200 Hz, which is sufficient to capture the force change. As shown in Fig. 8, the raw data read from the left and right sensor with the corresponding time was recorded.

By applying the equation aforementioned in Section 2.1, we obtained the separation force by summing up the left and right force measured. The calculated separation force over time is shown in Fig. 9.

As shown in Fig. 9, we have labeled the data plotted into 8 groups from a–h. The data from groups a–b was sampled from the base section of the CAD model as shown in Section 3.1. The data from groups c–d was sampled from the second section of the CAD model. The data from groups e–f was sampled from the third section of the CAD model. The data from groups g–h was sampled from the fourth section of the CAD model. Obviously, the data from groups a, c, e and g was obtained from a normal printing process without applying the vibration to the constrained glass and the data from groups b, d, f and h was obtained from

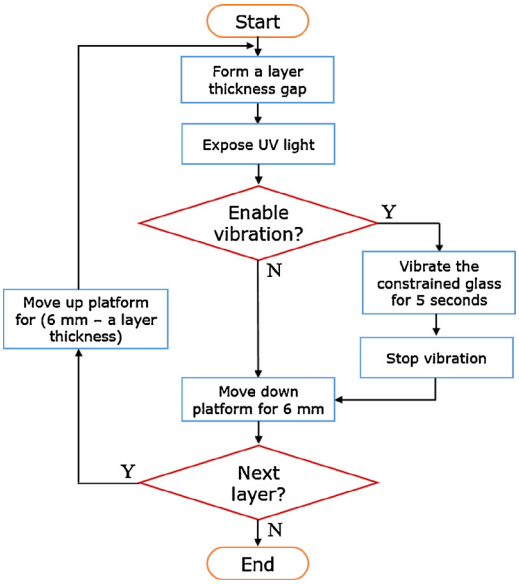

Fig. 7. The flow chart of designed printing process.

a vibration-assisted printing process with applying the vibration to the constrained glass.

By combining the data from groups a, c, e and g, we can learn that there is a decreasing trend of the separation force as the building area decreases in the normal printing process. However, the data from the groups b, d, f and h shows that the force here is independent with the building area in the vibration-assisted printing process. Specifically, the force in the groups b, d, f and h was caused by the upward and downward movement during the vibration rather than a separation force as it was measured in the normal printing process. It was determined by the amplitude of the vibration on the glass which was initially determined by the frequency of the input signal to the loudspeaker. We have figured out the amplitude of the vibration on the glass is ~300 μm. The method we used to measure the amplitude is described as follows. Firstly, we manually applied a pressure force at the point where a pulling force would be applied during vibration-assisted printing process as shown in Fig. 2-point A. Then we gradually increased the pressure force until the force value we read from the pressure sensor reached the value shown in Fig. 8a and b, respectively. The vertical displacement of point A we measured is treated as the amplitude of the vibration on the glass.

The Fig. 10 below shows a plot of the mean value of the data and standard deviation from groups of using normal printing process and vibration-assisted printing process, respectively. Here, we only care about the peak values generated during the separation process as shown in Fig. 9.

As shown in Fig. 10, by comparing the data got from the normal printing process and the vibration-assisted printing process, we can learn that as the building area increases, the vibration applied on the constrained glass with a certain frequency will help to reduce the separation force significantly. More importantly, unlike other methods aiming to reduce the separation force mentioned in Section 1.1, the proposed vibration-assisted printing process will not dramatically increase the mechanical construction complexity even if the required maximum building area increases.

As shown in Fig. 9b, we zoom in a representative place near the turning point between the normal printing process and the vibration-assisted printing process in the base section as shown in Fig. 9a. The polyline from point A to B in Fig. 9b denotes an increasing separation force which means the separation process began at the point A and reached the maximum separation force at point B at which moment the building surface was instantly separated from the constrained glass during the normal printing process. It caused a vertical displacement of the constrained glass as shown in Fig. 2. The separation force after the point B did not disappear immediately because of the damping effect of the spring as shown in Fig. 1 and mentioned in Section 2.1. The spring was under a compressed status from the point A to B. The total separation process lasted about 1 s in a normal separation process. After finishing building the first 40 layers in the base section, we enabled the vibration to help separate the building surface from the glass. As shown in Fig. 9b, the vibration compressed the spring from the point F to G due to the downward movement of the round flat pad as shown in Fig. 1 and then released the spring from the point G to H due to the upward movement of the round flat pad. This repeated upward and downward movement during the vibration caused a relatively dense wave pattern as shown in Fig. 9b. We can learn that the amplitude of the upward and downward movement is quite consistent from the overall view of the data sampled at different sections during the vibration-assisted printing process as shown in Fig. 9a.

3.4. Modeling of vibration based separation process

The dynamics of the system can be modeled as a forced vibration

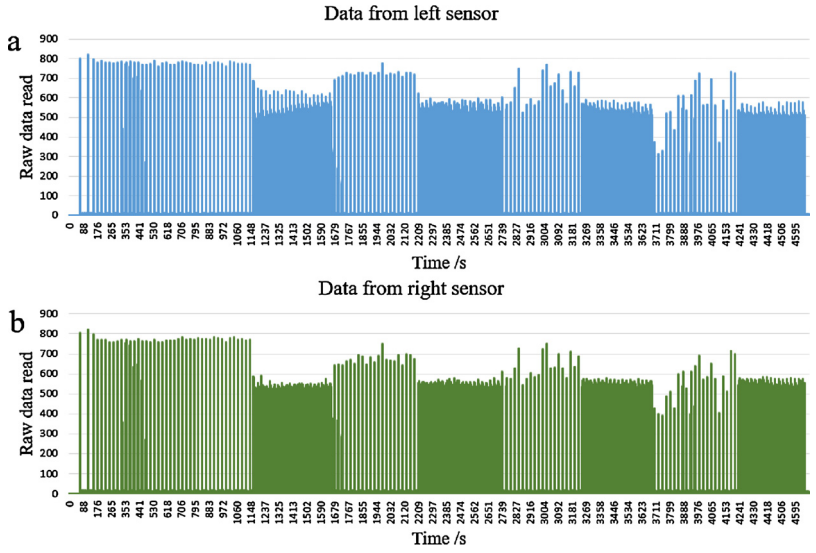

Fig. 8. (a) The raw data got from left sensor; and (b) the raw data got from right sensor.

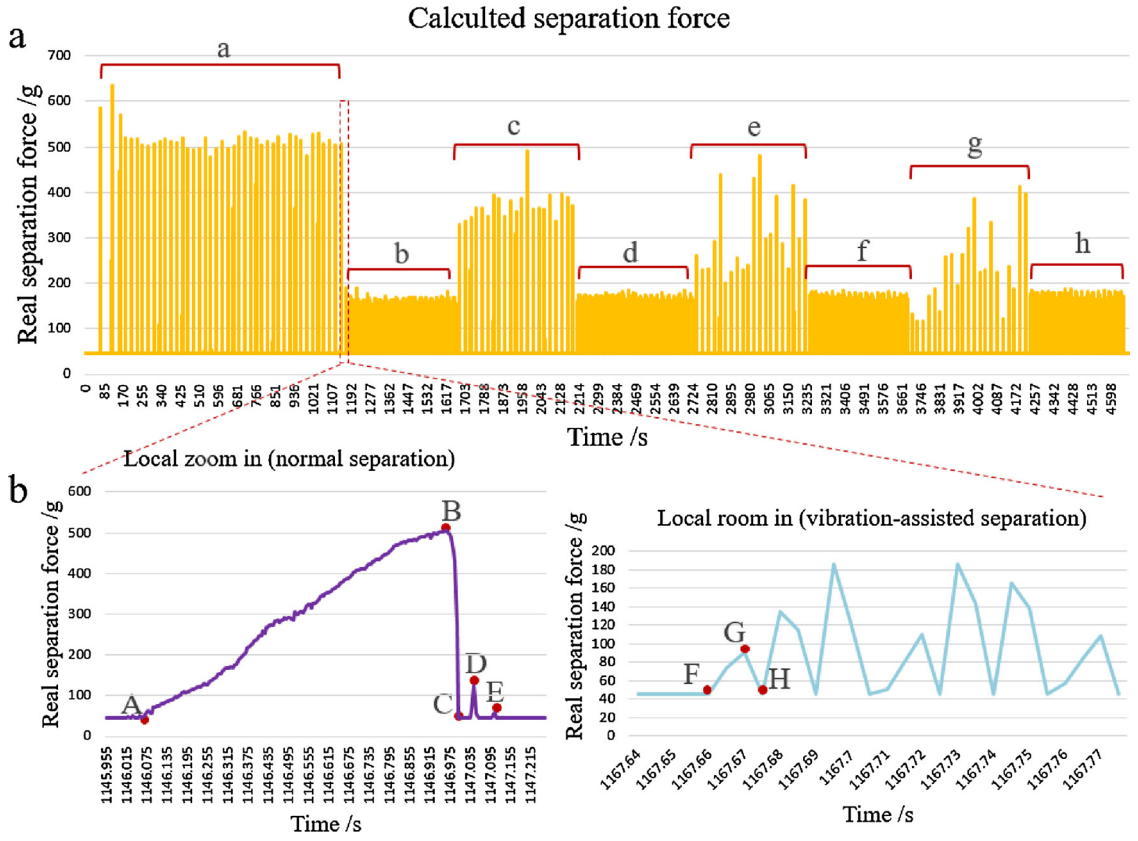

Fig. 9. Data visualization. (a) the calculated separation force over time; (b) a zoom-in view of the turning point.

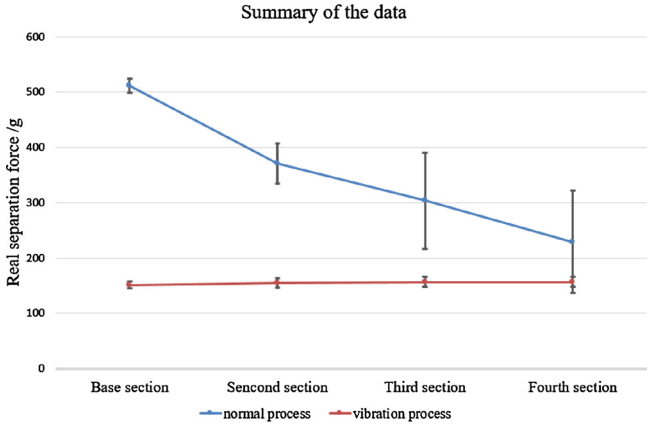

Fig. 10. A comparison of the separation force using different printing processes.

with damping:

$$m\ddot{x} + c\dot{x} + ku = F_0 sin(2\pi ft) \tag{4}$$

where m is the mass of the system, c is the damping coefficient, and k is the system's stiffness. The input vibration force is generated by a loudspeaker. F_0 and f are the amplitude and frequency of the loudspeaker's signal, respectively. The steady state solution [21] is

$$\begin{aligned} x &= A \cdot \sin(2\pi ft + \phi) \\ &= \frac{\frac{1}{2\pi}\frac{F_0}{\sqrt{km}}}{\sqrt{\left(f^2 - \frac{k}{4\pi^2 m}\right)^2 + \frac{c^2}{km} f^2}} \sin(2\pi ft + \phi) \end{aligned} \tag{5}$$

where the vibration amplitude A is subject to the vibration frequency f. Notice that the vibration approaches steady state just after several cycles.

In the proposed vibration-assisted system, the separation of the printed part with the constrained glass can be modeled as a fatigue crack propagation under a cyclical load. And P. Paris and F. Erdogan [22] demonstrated that the range of the stress intensity factor is the major parameter determining the crack propagation.

The stress intensity factor is modeled [23] as

$$K = \sigma\sqrt{\pi a} \bullet \theta(a) \tag{6}$$

where $\theta(a)$ is a geometry related coefficient, and σ is the stress load. In our setup, σ is the overall force divided by the contact area:

$$\sigma = \frac{kx}{(w-2a)^2} \tag{7}$$

where k is the system's stiffness, x is the vibration displacement, w is the length of the printed part, and a is the separation crack length,

According to Paris' Law [22], the growth rate of the crack length a w.r.t cycles N is predicted by

$$\frac{da}{dN} = C(\Delta K)^n \tag{8}$$

where C and n are material parameters, ΔK is the range of stress intensity factor applied on the edge of interface between the printed part and the constrained glass. This value is computed as:

$$\begin{aligned} \Delta K &= K_{max} - K_{min} \\ &= \sigma_{\max}\sqrt{\pi a} \bullet \theta(a) - \sigma_{\min}\sqrt{\pi a} \bullet \theta(a) \\ &= (\sigma_{\max} - \sigma_{\min})\sqrt{\pi a} \bullet \theta(a) \\ &= \frac{kA}{(w-2a)^2}\sqrt{\pi a} \bullet \theta(a) \\ &= \frac{1}{2\pi}\frac{F_0\sqrt{k/m}}{\sqrt{\left(f^2 - \frac{k}{4\pi^2 m}\right)^2 + \frac{c^2}{km} f^2}} \frac{\sqrt{\pi a} \bullet \theta(a)}{(w-2a)^2} \end{aligned} \tag{9}$$

By definition, the vibration frequency is $f = dN/dt$. Hence, the separation crack growth rate is

$$\frac{da}{dt} = \frac{da}{dN} \bullet \frac{dN}{dt} = C(\Delta K)^n f \tag{10}$$

This is the governing equation that predicts how the separation propagates with respect to time. This equation indicates that the separation speed is determined by the vibration signal's frequency f and amplitude F_0, system mass m, system stiffness k, material property C and n, and the geometry of the contact area. Also, from the equation, we can see that there exists an optimal frequency that can maximize the separation speed. This optimal frequency can be derived by differentiating the Eq. (10) w.r.t the frequency f. Any higher or lower frequency generates smaller range of stress intensity factor ΔK, and hence leads to a smaller crack progradation rate. Our experiments also verify this phenomenon.

Notice that, during the vibration, the displacement of the constrained glass was controlled within the vibration amplitude, which was ~300 μm in our experiments. Hence, the separation force maintains a small value regardless of the contact area size, and the experimental results shown in Fig. 10 also verifies this. Such small separation force enables our process to fabricate large area components efficiently.

In comparison, the maximal force in the conventional process without vibrations is largely affected by the contact area size. Various researches have illustrated that the separation force is highly determined by the contact area size [8,18,19]. Our experimental result in Fig. 10 also reveals that the separation force increases rapidly with the increase of contact area.

4. Results and discussion

4.1. The camera shot of the separation process

Multiple images as shown in Figs.11 and 12 were taken to record the surface separation process happened in a random layer chosen in the base section of the part from both normal printing process and vibration-assisted printing process. Noticed that the building platform moved down after the building surface had separated from the constrained glass in a vibration-assisted printing process as described in Fig. 7. To capture these images, we firstly recorded a video using an iPhone 8 Plus with a constant frame rate which was 60 Hz. Then we just extracted the frame images from the recorded video and got several images with a certain time interval which was 1/60 s. Although it will take ~1.67 s to separate the building surface from the constrained glass, it is still competitive among the existing separation methods as mentioned in Section 1.

4.2. The impact of the vibration to the dimensional accuracy

We have printed 10 same parts as designed in Section 3.1 and measured the dimensions along the X and Y directions in different sections. The measurement results match well with the designed dimensions. Since the vibration only causes the movement along the Z axis, the proposed vibration-assisted printing process does not affect the dimensional accuracy in the X and Y directions. The X-Y dimensional size of the printed part is only determined by the dimensional size of the projection pattern image. As long as the focus length of the projector was kept the same during the printing process, the dimensional accuracy in the X-Y directions can be guaranteed. For simplicity, we just care about the dimensional accuracy in the Z direction. As shown in the Table 1, we have measured the dimensions along the Z direction including the height of different individual sections of the printed parts. The measurement results are quite consistent with designed dimensions with the designed dimensions except the dimension in the base section. The dimensional error in the base section along the Z direction is caused by the over compression between the building platform and the top constrained glass. The measurement result along the Z direction also shows the fact that if the setup hardware is reliable, especially the membrane of the paper cone in the loudspeaker is highly recoverable which will not cause a permanent deformation during the vibration, the layer thickness in the Z direction for each layer printed can be guaranteed. It is not limited to use a loudspeaker to provide the vibration for the designed system, but the chosen method is low cost. Other alternative ways to generate more reliable vibration will be tried in our future work.

4.3. The impact of the vibration to the small features

As mentioned in Section 3.1, the amplitude of the vibration on the glass is much larger than the designed layer thickness which may potentially cause some unexpected damage to the original printed part, especially when there are some small features existing in the designed part. As shown in Fig. 13, we have designed a special case with some small features to verify this problem. The smallest diameter of the designed cylinders is 300 μm and the smallest wall thickness of the designed is 300 μm. As shown in Fig. 13, we have printed two parts with the same CAD design for comparison. One of them was printed using the normal printing process all the way and another one was printed using the proposed vibration-assisted printing process all the way. From the printed results, we can observe that both parts preserve most of the designed small features. The only big difference is about the printed column of cylinders which have the smallest designed diameter. The one printed by the normal printing process contains 7 of 10 designed cylinders while the other one printed by the vibration-assisted printing process only contains 2 of 10 designed cylinders. We have repeated the same comparison experiment for 5 times and the comparison results were similar with the one as shown in Fig. 13. This suggests that the proposed vibration-assisted printing process slightly affects some small features in the designed part.

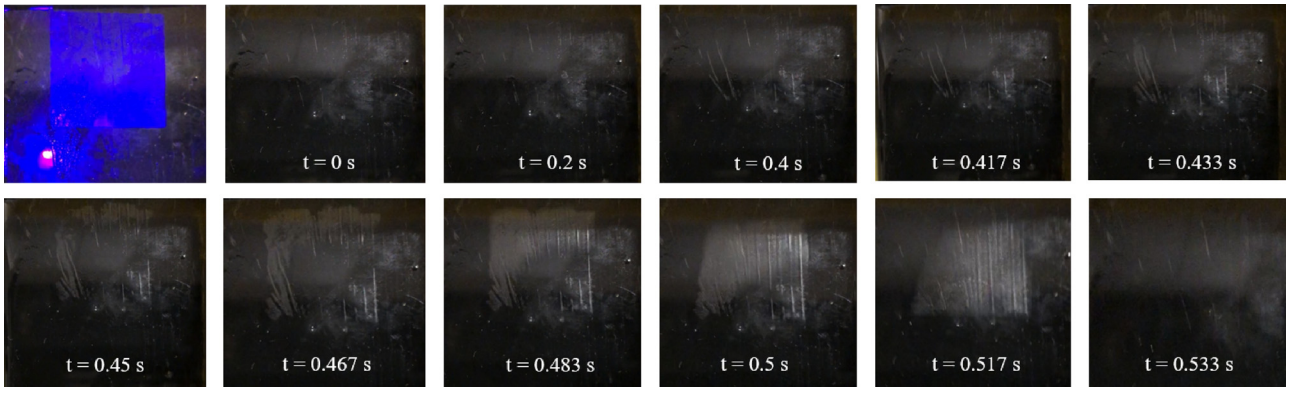

Fig. 11. The screen shots of a recorded normal separation process.

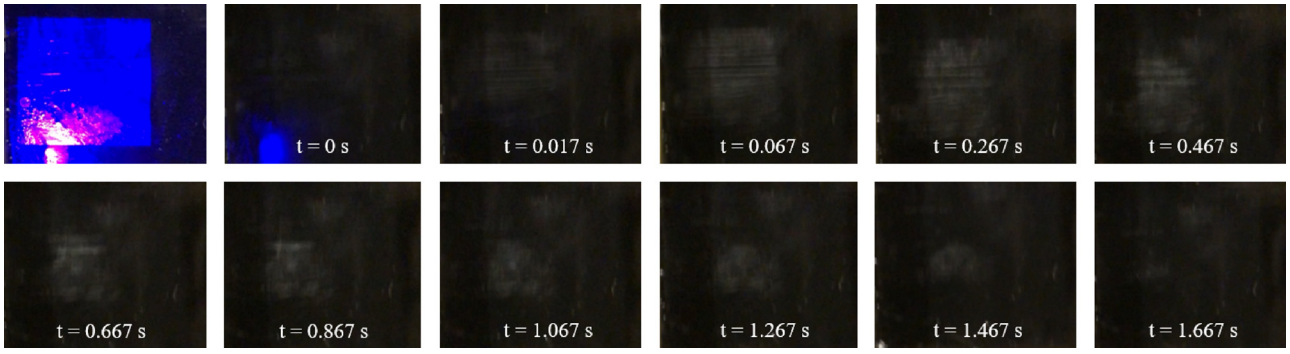

Fig. 12. The screen shots of a recorded vibration-assisted separation process.

Table 1
The dimensions along the *Z* direction.

	Height in the *Z* direction /mm	
	Designed size	Mean
Base section	6	5.32
Second section	4	3.97
Third section	4	3.92
Fourth section	4	3.95

4.4. Limitations and challenges

The presented vibration-assisted printing process has been demonstrated to have the ability to fabricate parts with a large area using our experimental setup. However, several issues and potential challenges have also been identified during the experiments that will be addressed in our future work.

- Damage to small features: Since the vibration-assisted process will cause a relatively big amplitude of the movement on the constrained glass. The unexpected damage caused by this upward and downward movement to the small features on the designed part cannot be avoided so far. To address this problem, we can adopt an adaptive vibration frequency during the printing process instead of using a constant vibration frequency. Thus, for parts have small features we can lower down the vibration frequency or disable the vibration to protect the small features. If there is a large cross-sectional area and small features existing in the same building layer, it will become a tradeoff problem. Another method to mitigate the damage is gradually increasing the vibration amplitude during each separation.
- Reliability of the hardware setup: Currently, we are using a loudspeaker to generate the vibration during our experiments. We haven't tested an even much larger printing area in our built setup. The reliability of the current setup is unknown. If the designed building area is much larger than the current one, the membrane of the paper cone on the loudspeaker may be permanently damaged. Thus, to build a more reliable setup to do further tests is necessary for a larger building area.

5. Conclusion

A new stereolithography process based on vibration assisted has been presented. Pressure sensors have been used to measure the separation force during the printing process. Controlled experiments have been implemented to do comparisons between using a normal printing process and the proposed vibration-assisted printing process. The data got from the sensor which was read in real time has been visualized and

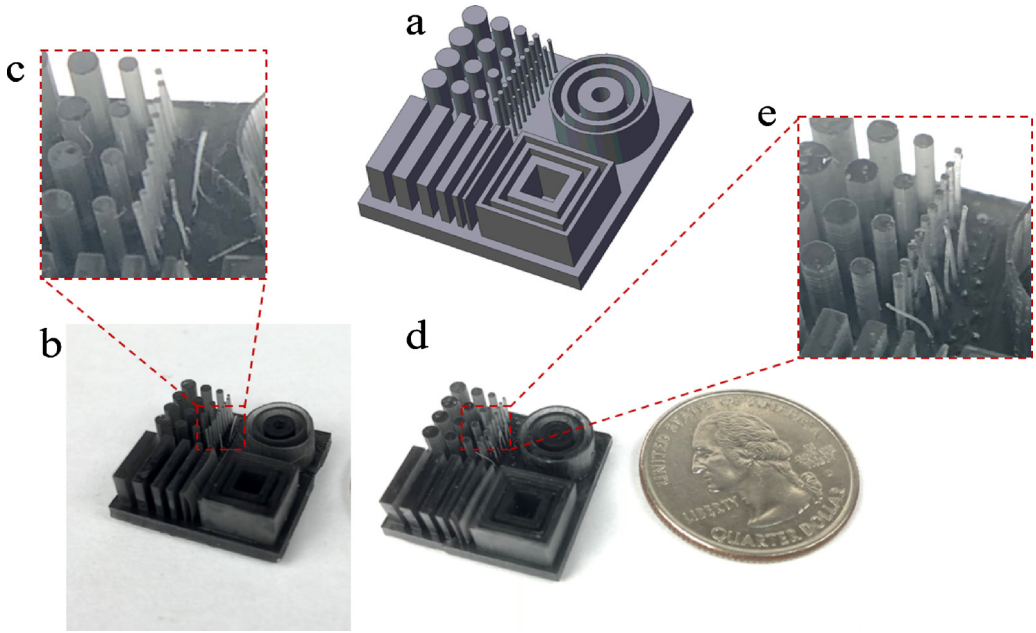

Fig. 13. (a) the designed CAD model for test; (b) part printed by the vibration-assisted printing process; (c) a close view of the small features in part (b); (d) part printed by the normal printing process; (e) a close view of the small features in part (d).

analyzed. An experimental prototype system has been built, which integrates various hardware and software components. Some representative test cases based on the prototyping system are presented to verify the capabilities of the proposed vibration-assisted printing process in significantly reducing the separation force and potentially building parts with a large cross-sectional area. The designed experimental system is based on a top-down SL process, but it can also be applied to the bottom-up SL process by simply modify the mechanical design.

Considerable work remains to mature the developed process and the correspondingly developed 3D printing system. Some future work that we are investigating includes: (1) refining the current setup to build parts with much larger cross-sectional area; and (2) developing an adaptive method to dynamically change the vibration frequency which is associated with the cross-sectional area change to protect the small features.

Acknowledgement

The work was partially supported by a National Science Foundation (NSF) grant (CMMI 1151191).

References

[1] Gibson I, Rosen DW, Stucker BAdditive. Manufacturing technologies. New York, NY: Springer; 2010.
[2] Pan Y, Chen Y. Smooth surface fabrication based on controlled meniscus and cure depth in micro-stereolithography. J Micro Nano- Manuf 2015;3(3):031001.
[3] Pan Y, Zhao X, Zhou C, Chen Y. Smooth surface fabrication in mask projection based stereolithography. J Manuf Process 2012;14(4):460–70.
[4] Melchels FP, Feijena J, Grijpma DW. A review on stereolithography and its applications in biomedical engineering. Biomaterials 2010;31(24):6121–30.
[5] Kruth JP, Leu MC, Nakagawa T. Progress in additive manufacturing and rapid prototyping. CIRP Ann Manuf Technol 1998;47(2):525–40.
[6] Mao Huachao, Leung Yuen-Shan, Li Yuanrui, Hu Pan, Wu Wei, Chen Yong. Multiscale stereolithography using shaped beams. J Micro Nano-Manuf 2017;5(4):040905.
[7] Zhou C, Chen Y, Yang Z, Khoshnevis B. Digital material fabrication using mask-image-projection based stereolithography. Rapid Prototyp J 2013;13:153–65.
[8] Huang YM, Jiang CP. On-line force monitoring of platform ascending rapid prototyping system. J Mater Process Technol 2005;159(2):257–64.
[9] Pan Y, Zhou C, Chen Y. A fast mask projection stereolithography process for fabricating digital models in minutes. J Manuf Sci Eng 2012;134(5):051011.
[10] Pan Y, Chen Y, Yu Z. Fast mask image projection based micro-stereolithography process for complex geometry. J Micro Nano-Manuf 2017;5(1):014501.
[11] Pan Y, Zhou C, Chen Y. Rapid manufacturing in minutes: the development of a mask projection stereolithography process for high-speed fabrication. Proceedings of the 2012 International Manufacturing Science and Engineering Conference. 2012. p. 405–14.
[12] Yong Chen, Huachao Mao, Xiangjia Li. "Mask Video Projection Based Stereolithography with Continuous Resin Flow." U.S. Patent Application No. 15/187,713.
[13] Jin Jie, Chen Yong. Highly removable water support for Stereolithography. J Manuf Process 2017;28:541–9.
[14] Bártolo PJ. Stereolithography. New York, NY: Springer; 2011.
[15] Liravi F, Das S, Zhou C. Separation force analysis and prediction based on cohesive element model for constrained-surface Stereolithography processes. Comput Aided Des 2015;69:134–42.
[16] Kovalenko I, Garan M, Shynkarenko A, Zelený P, Jirˇí S. Examining the relationship between forces during stereolithography 3D printing and geometric parameters of the model. MATEC Web Conf 2015;40. http://dx.doi.org/10.1051/matecconf/20164002005.
[17] Syao, K. “Stereolithography apparatus”, U.S. Patent Application 14/454,901, filed August 8, 2014.
[18] Ye Hang, Venketeswaran Abhishek, Das Sonjoy, Zhou Chi. Investigation of separation force for constrained-surface stereolithography process from mechanics perspective. Rapid Prototyp J 2017;23(4):696–710.
[19] Pan Yayue, He Haiyang, Xu Jie, Feinerman Alan. Study of separation force in constrained surface projection stereolithography. Rapid Prototyp J 2017;23(2):353–61.
[20] Tumbleston JR, Shirvanyants D, Ermoshkin N, Janusziewicz R, Johnson AR, Kelly D, Chen K, Pinschmidt R, Rolland JP, Ermoshkin A, Samulski ET, DeSimone JM. Continuous liquid interface production of 3D objects. Science 2015;347(6228):1349–52.
[21] Géradin Michel, Rixen Daniel J. Mechanical vibrations: theory and application to structural dynamics. John Wiley & Sons; 2014.
[22] Paris Paul Croce, Erdogan Fazil. A critical analysis of crack propagation laws. ASME 1963.
[23] Tada Hiroshi, Paris Paul C, Irwin George R. The stresss analysis of cracks. Handbook. Del Research Corporation; 1973.